Volume 6, Issue 4, 2016, 1411-1416 ISSN 2069-5837
Biointerface Research in Applied Chemistry
www.BiointerfaceResearch.com
Original Research Article Open Access Journal
Received: 27.04.2016 / Revised: 30.06.2016 / Accepted: 15.07.2016 / Published on-line: 20.07.2016

A designed Al_2O_3-SiO_2-MgO nanocomposite as a highly efficient adsorbent for removing of methyl orange from aqueous solution

M. Iranpour Mobarakeh [1], A. Saffar-Teluri [1,2,*], S.A. Hassanzadeh-Tabrizi [1]
[1]Advanced Materials Research Center, Faculty of Materials Engineering, Najafabad Branch, Islamic Azad University, Najafabad, Iran
[2]Department of Chemistry, Faculty of Science, Najafabad Branch, Islamic Azad University, Najafabad, Iran
*corresponding author e-mail address: ***a.saffar13@gmail.com***

ABSTRACT
In this study, Al_2O_3-SiO_2 and Al_2O_3-SiO_2-MgO nanocomposites were synthesized by sol-gel method. The nanocomposites were characterized by FT-IR, STA, XRD, FE-SEM, EDAX, TEM, BET and zeta potential analysis. The result of zeta potential showed that the surface of Al_2O_3-SiO_2-MgO nanocomposite had the positive charge, while that of Al_2O_3-SiO_2 had the negative charge. The nanocomposites were applied as an adsorbent for removing of methyl orange model dye and the effect of adsorbent dosage and dye concentration were studied.
KEYWORDS: *Nanocomposite, sol-gel, adsorbent, removal.*

1. INTRODUCTION
The color effluents coming from different industries into water environment have a great influence on photosynthetic activity in aquatic biota. Since these dyes are stable, recalcitrant, colorant and toxic, their release into the environment poses serious environmental, aesthetical and health threats. Thus, removal of organic effluents is very important for protection of our environment [1]. Coagulation and flocculation, oxidation or ozonation, membrane separation, and adsorption are the conventional methods that are used in dyes removal from wastewater [3–9]. Adsorption processes have been reported to be the low-cost promising alternatives for the treatment of dyes that present in wastewater. The use of activated carbons, modified clays, polymeric resins, waste materials, and zeolites as the dyes adsorbents have also been described [10]. Activated carbon is the most prevailing adsorbent for this process because of its high surface area, high adsorption capacity, and high degree of surface reactivity; however, it is expensive and must be regenerated on a regular basis. Inorganic supports present several advantages with respect to activated carbon, including better mechanical stability and a higher concentration of chelating groups on the surface, and they are often much cheaper than their organic counterparts.

Al_2O_3-SiO_2 mixed oxides, or composites of them, are ceramic materials that are widely used as catalysts and an inorganic supports [10–17]. Clay minerals [10], zeolites [11, 15], mullite [13], and SiO_2–Al_2O_3 catalysts are examples of materials where the existence of Al-O-Si bond structures or SiO_2–Al_2O_3 interfaces controls their final performance for the desired application. The reason for choosing these particular mixed oxides was the properties such as low thermal expansion and conductivity, low dielectric constant, excellent creep resistance, robust chemical and thermal stability, good high temperature strength and oxidation resistance [16].

Metal oxides have potential applications in water treatment due to their high surface area added to low production and regeneration costs. Among large family of metal oxides, magnesium oxide (MgO) is an interesting multifunctional and an exceptionally important material used in catalysis [18], toxic-waste remediation or as an additive in refractory, paint and superconducting products as well as for fundamental and application studies [19]. Also it has been used as bactericides and adsorbents. MgO in particular has shown great promise as a destructive adsorbent for toxic chemical agents [20]. MgO is mainly obtained by the thermal decomposition of magnesium hydroxide or carbonate, sol–gel process, spray pyrolysis, sonochemical synthesis and hydrothermal reaction [19, 21–23]. The MgO morphology and particle size were found to depend on the preparation conditions such as pH, gelling agent, calcination rate and temperature.

In this paper, Al_2O_3-SiO_2-MgO nanocomposites with different amounts of MgO (20, 40 and 60%) were synthesized by sol-gel method and characterized by FT-IR spectroscopy, STA, XRD, FE-SEM, EDS, TEM and zeta potential. These nanocomposites were used as the adsorbent for removing methyl orange from the aqueous solution. Methyl orange (MO) is a typical water-soluble anionic dye which has harmful effects on living organisms in a short period of exposure [24].

2. EXPERIMENTAL SECTION
2.1. Materials and the synthesis of nanocomposites.
All the reagents were purchased from Merck and Aldrich and used without further purification. Al_2O_3-SiO_2-MgO nanocomposites with 20, 40 and 60 wt% of MgO were synthesized using sol-gel approach. First, tetraethylorthosilicate (TEOS) was diluted in ethanol and water. Then, the necessary amount of HCl

(37%) was added to the mixture and refluxed in 75 °C for 2h (TEOS: C_2H_5OH: H_2O: HCl molar ratio was 1: 22: 13: 7.9×10^{-4}). Afterwards, the dissolved magnesium nitrate ($Mg(NO_3)_2.6H_2O$) and aluminum nitrate ($Al(NO_3)_3.9H_2O$) in ethanol was added to the mixture and refluxed at 75 °C for another 2h. The resulting mixture was aged at room temperature for 24h and dried in oven at 120 °C for 24h. Then, they were calcined to 500 °C at the heating rate of 8 °C/min and once 500 °C was reached, they were kept at this temperature for 12h.The nominal content of MgO was 0, 20, 40 and 60 wt %, and the corresponding nanocomposites were denoted as AlSiM0, AlSiM20, AlSiM40 and AlSiM60, respectively.

2.2. Characterization.

Fourier transform infrared (FT-IR) spectroscopy was performed using a Jasco FT/IR-3600 FT-IR spectrometer. The phase and crystallinity were characterized using a Philips x'pert X-ray diffractometer with Cu- Kα radiation in the 2θ range of 10–80◦. Zeta potential analysis of 60 wt% nanocomposite dispersed in water was achieved using a Malvern Zetasizer Nano instrument at 25°C. FE-SEM and EDAX were taken by a SIGMA VP Field Emission Scanning Electron Microscopy. The weight change of the composite samples was measured using the TGA/DTA simultaneous thermal analyzer apparatus of METTLER TGA/SDTA 851E under a flow of dry air. Specific surface area was carried out using micro metrics adsorption equipment (BELSORP instrument, Japan).

2.3. Adsorption experiments.

The dye removal experiment was conducted at room temperature as batches. Typically, a stock solution (1 g/L) of MO dye was prepared in deionized water, then experimental solutions with different initial concentrations (10–40 mg/L) were obtained by successive dilutions. The required amount of AlSiM nanocomposite was added into the 10 ml dye solution and stirred for the predefined time. After that the suspension was centrifuged and supernatant was analyzed by UV–Vis spectra to calculate the residual dye concentration. The removal of dye percentage (R) was calculated using equation:

$$R= \{(C_0 - C_t)/C_0\} \times 100$$

where C_0 is initial concentration and C_t is the dye concentration at time t.

3. RESULTS SECTION

3.1. FTIR analysis.

Figure 1 presents the FTIR spectra of AlSiM60 sample before (a) and after (b) calcinating at 500 °C.

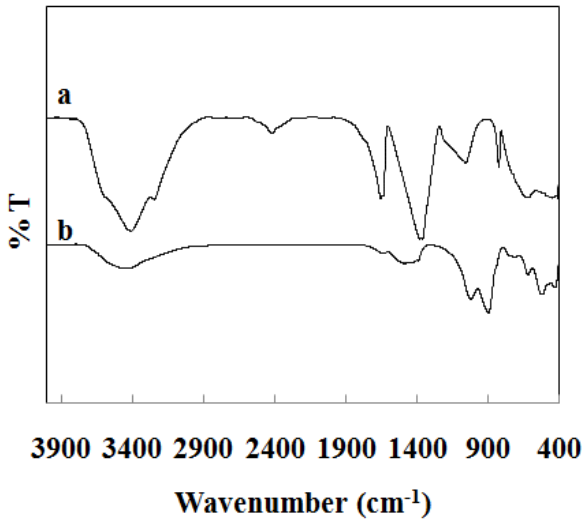

Figure 1. FTIR spectra of AlSiM60 sample before (a) and after (b) calcinating at 500 °C.

In Figure 1a, the adsorption peaks at 3410 cm^{-1} and 1654 cm^{-1} are attributed to the stretching vibration and bending vibration of O-H group for water, respectively. The absorption at 2416 cm^{-1} could be because of the existence of CO_2 molecular in air. The presence of nitrate ion in the sample is confirmed using a very strong band at 1380 cm^{-1} and a sharp peak at 824 cm^{-1}, which are due to the asymmetric NO_3^- stretching vibration [25]. The absorption peak of Al–O stretching vibration in the range of 1000–1200 cm^{-1} could not be resolved due to its overlap with the absorption peak of Si–O–Si stretching vibration in the range of 1000–1130 cm^{-1}. Also, the peaks between 420 and 618 cm^{-1} correspond to the Al-O and Mg-O bond vibrations [26-30]. The individual peaks corresponding to Mg-O bond and Al-O bond are obtained only when the sample is calcined at 500 °C. In Figure 1b, the absorption peaks of 427 cm^{-1} and 517 cm^{-1} are attributed to Mg-O vibration, whereas the peaks obtained at 619 cm^{-1} and 712 cm^{-1} indicate Al-O bond vibrations. There is also a band in 898 cm^{-1} and 1023 cm^{-1} due to the Al-O-Al and Si-O-Si bond stretching vibrations. The stretching vibration and bending vibration of O-H group for water appears at 3444 cm^{-1} and 1634 cm^{-1}, respectively.

3.2. X-ray diffraction analysis.

The room temperature X-ray diffraction (XRD) patterns of AlSiM0, AlSiM20, AlSiM40 and AlSiM60, and also the calcined AlSiM60 at 580 °C, are presented in Figure 2 a-e, respectively.

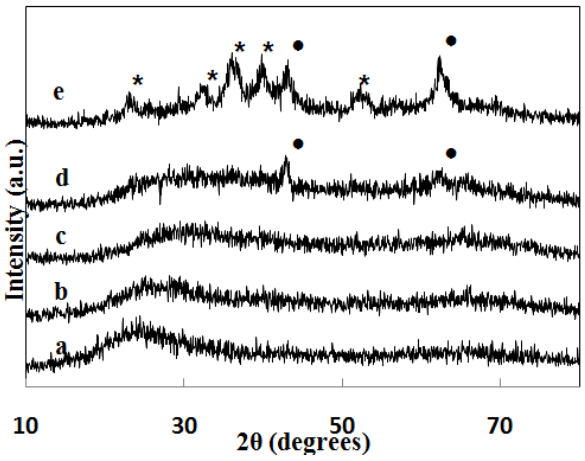

Figure 2. XRD patterns of AlSiM0 (a), AlSiM20 (b), AlSiM40 (c), AlSiM60 (d) and calcinated AlSiM60 at 580 °C (e).

The solid AlSiM0 displays the characteristic spectral profile of an amorphous structure at the 2θ = 23 for Al_2O_3-SiO_2. Comparison with the spectrum of AlSiM0, no peak was observed for AlSiM20 and AlSiM40, as shown in Figure 2a-c. With increasing the MgO content to 60 wt%, two peaks appeared at 2θ = 43.22° and 62.98°, which can be indexed to the structure of MgO (JCPDS card No: 78-0430). According to the XRD result in Figure 2e, calcining the precursor of AlSiM60 at 580 °C for 12h caused to form $MgAl_2O_4$ and Mg_2SiO_4. Since our aim in this study was the formation of Al_2O_3-SiO_2-MgO nanocomposites, therefore we selected 500°C for calcining the samples.

3.3. Thermal analysis.

TG-DTA result of the AlSiM60 precursor is shown in Figures 3a and 3b.

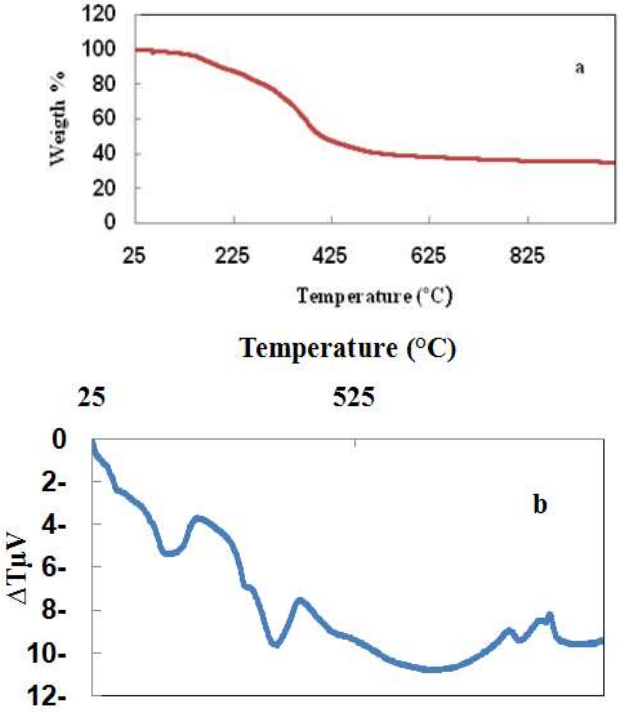

Figure 3. TG (a) and DTA (b) patterns of the precursor of AlSiM60 sample.

The process of weight loss can be divided into two steps. The endothermic peak between 25 and 225 °C on DTA, accompanied by 13% of weight loss observed in this first step on TG curve, is attributed to the desorption of water and solvent (which may be physical or chemical adsorption on the interparticle surface of the sample). The second step from 325 to 425 °C with the main weight loss of about 30%, accompanied by a endothermic peak at 375 °C, can correspond to the weight loss of dehydroxylation caused by breaking Si-OH and Al-OH as well as the calcination of MgO precursor. The two exothermic peaks at 700-825 °C and 825-925 °C on DTA are attributed to the formation of the crystalline phase of $MgAl_2O_4$ and Mg_2SiO_4 .

FE-SEM images and EDAX analysis of samples AlSiM0, AlSiM20, AlSiM40 and AlSiM60 are presented in Figure 4 a-h.

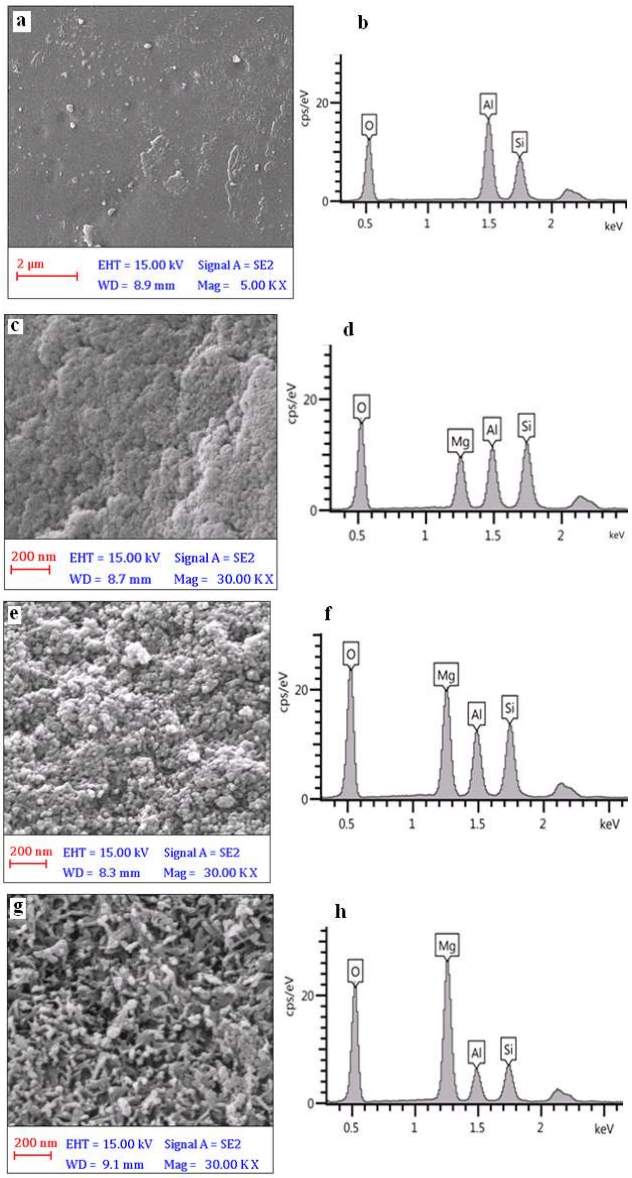

Figure 4. FE-SEM images and EDAX patterns of AlSiM0 (a and b), AlSiM20 (c and d), AlSiM40 (e and f) and AlSiM60 (g and h).

Three types of morphology (uniform (a), spherical-like (c and e) and bent rod-like (g)) can be seen in the FE-SEM images. Surface morphology of AlSiM20, AlSiM40 and AlSiM60 samples are different from the AlSiM0 as would expected due to formation of MgO in nanocomposites. The AlSiM0 nanocomposite has a uniform structure, while adding MgO to nanocomposites causes to form homogeneous spherical-like and bent rod-like particles. In all of images the MgO nanoparticles exist in the nanocomposites with almost uniform distribution.

The EDAX patterns are performed to identify the elemental composition of the nanocomposites. From the corresponding EDAX spectra, AlSiM0, AlSiM20, AlSiM40 and AlSiM60 nanocomposites are composed of Al, Si and O elements (Figure 4b) and of Al, Si, O, and Mg elements (Figures 4d, 4f and 4h), respectively. These results are in good agreement with the XRD analysis and strongly prove that the MgO is successfully mixed with Al_2O_3-SiO_2 matrix.

In order to obtain the crystallite size of nanocomposite, the TEM image of AlSiM60 is shown in Figure5. Based on Figure 5, nanoparticles size distribution is continuous between the minimal diameter (about 5 nm) and the maximal diameter (about 80 nm).

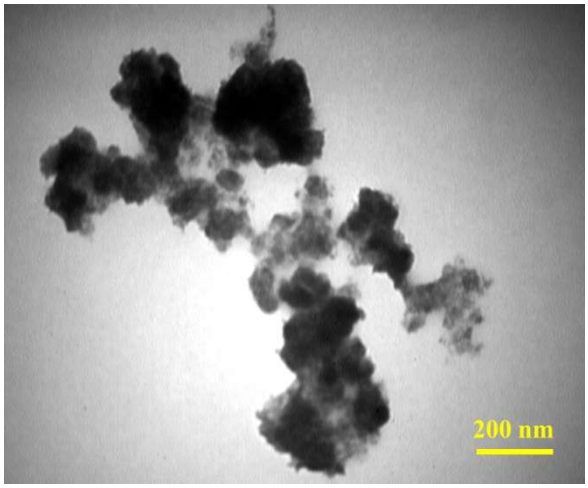

Figure 5. TEM image of AlSiM60.

3.4. Effect of dosage and type of adsorbent.

Figure 6 shows the effect of adsorbent dosage (0.001, 0.003, 0.007 and 0.01 g) and type of adsorbent (AlSiM0, AlSiM20, AlSiM40 and AlSiM60) on the percentage removal of 10 mg/L MO solution, without any change on the solution pH.

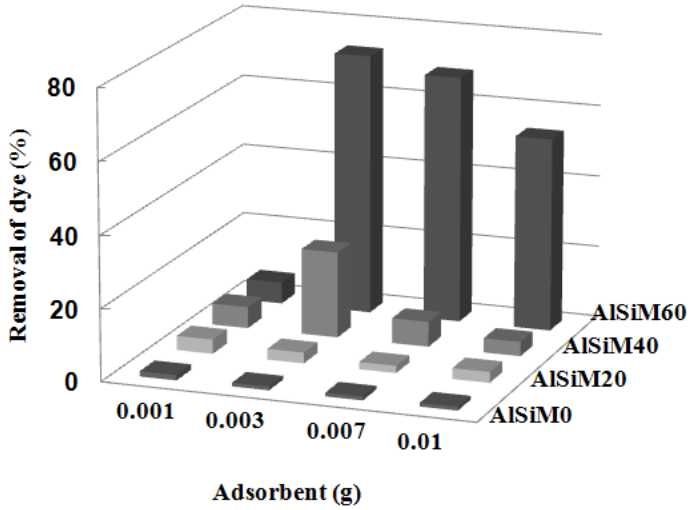

Figure 6. Effect of adsorbent dosage and type of adsorbent on the percentage removal of 10 mg/L MO solution.

The removal capacity of nanocomposites enhanced with the increase of MgO content from 20 to 60 wt%. The AlSiM60 adsorbent, that has the highest MgO content, exhibited the highest removal capacity. Based on Figure 6, AlSiM60 dosage increased from 0.001 to 0.003 g, the removal efficiency of MO ions increased significantly from 6 to 73%. However, the higher adsorbent dose results in a lower removal capacity of AlSiM60 (54%). It is believed that at the low adsorbent dosage the dispersion of AlSiM60 nanoparticles in aqueous solution is better, that is, all of the active sites on the adsorbent surface are entirely uncovered which could accelerate the approachability of MO molecules to a large number of the adsorbent active sites. Thus, the adsorption on the surface active sites is saturated quickly, performing a high removal capacity. On the other hand, at higher adsorbent dosage, the accessibility of adsorbent active sites with higher energy decreases and a larger fraction of the active sites with lower energy become occupied; leading to a decrease in adsorption capacity [31]. Furthermore, increasing adsorbent dosage enhances the chance of collision between adsorbent nanoparticles and hence creates particle aggregation, thereby inducing a decline in the total surface area and an increase in the diffusion path length, which both result in a decrease in the amount of MO from aqueous solution [32]. Therefore, 0.003 g of AlSiM60 was chosen as the optimal dosage for this process.

The effect of initial MO concentration on the percentage removal of the dye by keeping the adsorbent constant (0.003g) is shown in Figure 7.

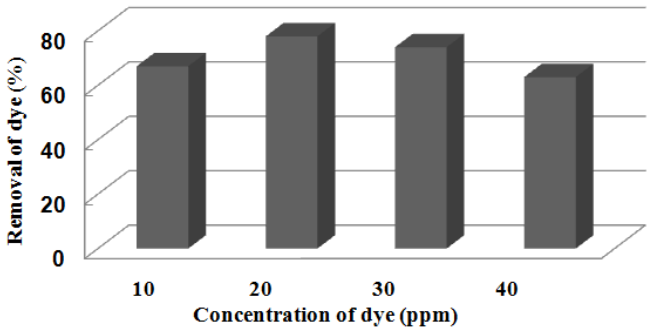

Figure 7. Effect of different initial MO concentration on the percentage removal of the dye (adsorbent dosage = 0.003g).

The percentage removal for 10, 20, 30 and 40 mg/L initial concentration was 67, 78, 74 and 63% after 90 min of adsorption, respectively. The percentage of dye removal increased from 67 to 78% with the increase in MO concentration from 10 to 20 mg/L and then decreased to 74 and 63% for 30 and 40 mg/L of dye concentration, respectively. The relative increase in the loading capacity of the sorbent with increasing MO concentration to 20 mg/L is probably due to the interaction between the dye and adsorbent, which provides the vital driving force to defeat the resistance to the mass transfer of MO ions between the aqueous and AlSiM60 [33]. On the other hand, the lower removal efficiency of AlSiM60 at high MO initial concentration (30 and 40 mg/L) could be related to the low ratio of initial mole numbers of MO to the available active sites on the surface area; therefore, the fractional adsorption is dependent on the initial concentration [34].

In order to confirm the above results, the structures of the nanocomposites were studied by determining of zeta potential and BET technique. Zeta potential of AlSiM60 nanocomposite is shown in Figure 8. It shows the surface of AlSiM60 has a positive charge of about 3.25 mV while that of MgO and AlSiM0 have negative charge of -1.25 and -15 mV, respectively (which are not shown here).

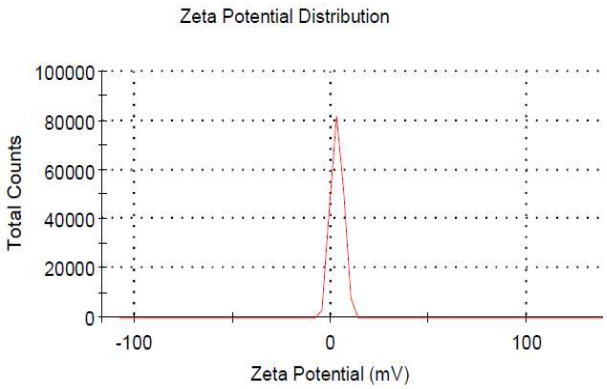

Figure 8. Zeta potential of the AlSiM60 nanocomposite.

The results of BET measurements for nanocomposites are presented in Table 1. The AlSiM0 nanocomposite has a low BET

surface area (63 m^2/g). The surface area of the AlSiM20, AlSiM40 and AlSiM60 nanocomposites (141, 148 and 151 m^2/g, respectively) gradually increased with increasing MgO.

Based on Figure 4, Table 1, Figure 6 and Figure 7, high adsorption capacity of AlSiM60 can be due to the existence of a larger amount of uncovered and covered MgO on the surface and in the structure of Al_2O_3-SiO_2 in comparison with other nanocomposites.

Table 1. BET measurements results for different nanocomposites.

Sample	Surface area (m^2/g)
AlSiM0	63
AlSiM20	141
AlSiM40	148
AlSiM60	151

4. CONCLUSIONS

Al_2O_3-SiO_2-MgO nanocomposites with different amount of MgO (20, 40 and 60%) were synthesized by sol-gel method and characterized by FT-IR, STA, XRD, FE-SEM, EDAX, TEM, BET and zeta potential analysis. These nanocomposites were used as adsorbent for the removal of methyl orange from aqueous solution. The nanocomposite with 60% of MgO was chosen an effective adsorbent. The optimum dosage and dye concentration were found to be 0.003g and 20 mg/L, respectively.

5. REFERENCES

[1] Lewis D.L., Garrison A.W., Wommack K.E., Whittemore A., Steudler P., Melillo J., Influence of environmental changes on degradation of chiral pollutants in soils, *Nature,* 401, 898–901, **1999.**

[2] Avlonitis S.A., Poulios I., Sotiriou D., Pappas M., Moutesidis K., Simulated cotton dye effluents treatment and reuse by nano filtration, *Desalination*, 221, 259–267, **2008.**

[3] Yue Q.Y., Gao B.Y., Wang Y., Zhang H., Sun X., Wang S.G., Gu R.R., Synthesis of polyamine flocculants and their potential use in treating dye wastewater, *Journal of Hazardous Materials*, 152, 221–227, **2008.**

[4] Wang S., A comparative study of Fenton and Fenton-like reaction kinetics in decolourisation of wastewater, *Dyes and Pigments*, 76, 714–720, **2008.**

[5] Sundrarajan M., Vishnu G., Joseph K., Ozonation of light-shaded exhausted reactive dye bath for reuse, *Dyes and Pigments*, 75, 273–278, **2007.**

[6] Liu J., Ma S., Zang L., Preparation and characterization of ammonium functionalized silica nanoparticle as a new adsorbent to remove methyl orange from aqueous solution, *Applied Surface Science*, 265, 393–398, **2013.**

[7] Tajizadegan H., Jafari M., Rashidzadeh M., Saffar-Teluri A., A high activity adsorbent of ZnO–Al2O3 nanocomposite particles: synthesis, characterization and dye removal efficiency, *Applied Surface Science*, 276, 317–322, **2013.**

[8] Deligeer W., Gao Y.W., Asuha S., Adsorption of methyl orange on mesoporous α-Fe_2O_3/SiO_2 nanocomposites, *Applied Surface Science*, 257, 3524–3528, **2011.**

[9] Anbia M., Asl Hariri S., Ashrafizadeh S.N., Adsorptive removal of anionic dyes by modified nanoporous silica SBA-3, *Applied Surface Science*, 256, 3228–3233, **2010.**

[10] Chen J.P., Wu S., Acid/base-treated activated carbons: characterization of functional groups and metal adsorptive properties, *Langmuir*, 20, 2233–2242, **2004.**

[11] Vaccary V., Clays and catalysis: a promising future, *Applied Clay Science*, 14, 161–198, **1999.**

[12] Arshadi M., Ghiaci M., Gil A., Schiff base ligands immobilized on a nanosized SiO2–Al2O3 mixed oxide as adsorbents for heavy metals, *Industrial and Engineering Chemistry Research*, 50, 13628–13635, **2011.**

[13] Sanchez-Soto P.J., Perez-Rodríguez J.L., Sobrados I., Sanz J., Influence of grindingin pyrophyllite-mullite thermal transformation assessed by 29Si and 27Al MAS NMR spectroscopies, *Chemistry of Materials*, 9, 677–684, **1997.**

[14] Arshadi M., Ghiaci M., Ensafi A.A., Karimi-Maleh H., Steven L. Suib, Oxidation of ethylbenzene using some recyclable cobalt nanocatalysts: the role of linker and electrochemical study, *Journal of Molecular Catalysis A: Chemical,* 338, 71–83, **2011.**

[15] Ensafi A.A., Karimi-Maleh H., Ghiaci M., Arshadi M., Characterization of Mnnanoparticles decorated organofunctionalized SiO_2–Al_2O_3 mixed-oxide as a novel electrochemical sensor: application for the voltammetric determination of captopril, *Journal of Materials Chemistry*, 21, 15022–15030, **2011.**

[16] Arshadi M., Ghiaci M., Highly efficient solvent free oxidation of ethylbenzene using some recyclable catalysts: the role of linker in competency of manganese nanocatalysts, *Applied Catalysis A: General,* 399, 75–86, **2011.**

[17] Arshadi M., Ghiaci M., Rahmanian A., Ghaziaskar H., Gil A., Oxidation of ethylbenzene to acetophenone by a Mn catalyst supported on a modified nanosized SiO_2/Al_2O_3 mixed-oxide in supercritical carbon dioxide, *Applied Catalysis B: Environmental*, 119–120, 81–90, **2012.**

[18] Tsuji H., Yagi F., Hattori H., Kita H., Self-Condensation of N-butyraldehyde over solid base catalysts, *Journal of Catalysis*, 148, 759–770, **1994.**

[19] Makhluf S., Dror R., Nitzan Y., Abramovich Y., Jelinek R., Gedanken A., Microwave-assisted synthesis of nanocrystalline MgO and its use as a bacteri-ocide, *Advanced Functional Materials*, 15, 1708–1715, **2005.**

[20] Mishakov A.F., Bedilo R.M., Richards V.V., Chesnokov A.M., Volodin V.I., Zaikovskii R.A., Buyanov K.J., Klabunde, Nanocrystalline MgO as a dehydro halogenation catalyst, *Journal of Catalysis*, 206, 40–48, **2002.**

[21] Xu B.Q., Wei J.M., Wang H.Y., Sun K.Q., Zhu Q.M., Nano MgO: novel preparation and application as support of Ni catalyst for CO_2 reforming of methane, *Catalysis Today*, 68, 217–225, **2001.**

[22] Choi H.S., Hwang S.T., Sol–gel-derived magnesium oxide precursor for thin-film fabrication, *Journal of Materials Research*, 15, 842–845, **2000.**

[23] Ranjit K.T., Klabunde K.J., Solvent effects in the hydrolysis of magnesium methoxide, and the production of nanocrystalline magnesium hydroxide. Anaid in understanding the formation of porous inorganic materials, *Chemistry of Materials*, 17, 65–73, **2005.**

[24] Mohammadi N., Khani H., Gupta V.K., Amereh E., Agarwal S., Adsorption process of methyl orange dye onto mesoporous carbon material – kinetic and thermodynamic studies, *Journal of Colloid and Interface Science*, 362, 457–462, **2011.**

[25] Ferdousi A., Podder J., Structural, Optical, electrical and thermal characterizations of pure and L-alanine doped ammonium dihydrogen phosphate crystals, *Journal of Crystallization Process and Technology*, 1, 18-25, **2011.**

[26] Pattersona M.J., Angovea D.E., Canta N.W., Nelsonb P.F., The formation of benzene and chlorobenzene during the oxidation of toluene over rhodium-based catalysts, *Applied Catalysis B: Environmental*, 20, 123–131, **1999.**

[27] Adamczyk A., The spectroscopic studies of glasses in the BPO_4($GaPO_4$)–SiO_2 system, *Journal of Molecular Structure*, 614, 127-132, **2002.**

[28] Machado G.S., Castroa K.A.D.F., Lima O.J., Nassarb E.J., Ciuffib K.J., Nakagaki S., Aluminosilicate obtained by sol–gel process as support for an anionic iron porphyrin: Development of a selective and reusable catalyst for oxidation reactions, *Colloids and Surfaces A: Physicochemical and Engineering Aspects*, 349, 162-169, **2009.**

[29] Chandradass J., Jun B., Bae D.S., Effect of different fuels on the alumina–zirconia nanopowder synthesized by sol–gel auto combustion method, *Journal of Noncrystalline Solids*, 354, 3085–3087, **2008.**
[30] Crisan M., Jitianu A., Zaharescu M., Mizukami F., Niwa S.I., Sol-gel mono- and poly-component nanosized powders in the Al_2O_3–TiO_2–SiO_2–MgO System, *Journal of dispersion of dispersion science and technology*, 24, 13144, **2003.**
[31] Huang J.H., Liu Y.F., Wang X.G., Selective sorption of tannin from flavonoids by organically modified attapulgite clay, *Journal of Hazardous Materials*, 160, 382–387, **2008.**
[32] Zhao D., Sheng G., Hu J., Chen C., Wang X., The adsorption of Pb(II) on Mg_2Al layered double hydroxide, *Chemical Engineering Journal*, 171, 167–174, **2011.**
[33] Aksu Z., Kabasakal E., Batch adsorption of 2,4-dichlorophenoxy-acetic acid (2,4-D) from aqueous solution by granular activated carbon, *Separation and Purification Technology*, 35, 223–240, **2004.**
[34] Ni Z.M., Xia S.J., Wang L.G., Xing F.F., Pan G.X., Treatment of methyl orange by calcined layered double hydroxides in aqueous solution: adsorption property and kinetic studies, *Journal of Colloid and Interface Science*, 316, 284–291, **2007.**

6. ACKNOWLEDGEMENTS

We gratefully acknowledge for financial support from the Research Council of Islamic Azad University of Najafabad Branch.

© 2016 by the authors. This article is an open access article distributed under the terms and conditions of the Creative Commons Attribution license (http://creativecommons.org/licenses/by/4.0/).